THE EFFECT OF POROSITY ON THE MICROSTRUCTURAL DAMPING RESPONSE OF A 6061 ALUMINUM ALLOY

J. Zhang[1], M. N. Gungor[2] and E. J. Lavernia[1]

[1] Department of Mechanical and Aerospace engineering
University of California at Irvine
Irvine, CA 92717

[2] Westinghouse Science and Technology Center
1310 Beulah Road, Pittsburgh, PA 15235

ABSTRACT

There is a strong experimental evidence suggesting that the presence of pores or cavities in a microstructure may play an important role in the damping response of a material. The present paper reports on the results of a systematic study of the effects of micrometer-sized pores on the damping response of 6061 aluminum alloy. Spray atomization and deposition processing was selected for the present study as a result of its ability to produce a material with a pre-determined amount of non-interconnected, micrometer-sized pores or cavities. Furthermore, by using this synthesis approach, the amount and distribution of pores present in the material may be systematically altered through variations in the processing parameters. 6061 Al alloy was selected for the present study because it has been widely used in structural applications, and because its damping behavior has been studied previously. The damping measurements were accomplished on cantilever beam specimens by using the free vibration decay logarithmic decrement and the resonant vibration half band width techniques. The present results suggest that there is a correlation between the damping response of the material and the amount of porosity present in the microstructure. The damping capacity, logarithmic decrement δ, of the as-spray deposited material increased from 1.8 to 2.9% as the amount of porosity increased from 4 to 10%. A correlation between the magnitude of the damping capacity and the average pore diameter was also noted. Overall, the damping response of the spray deposited materials is higher than that reported by other investigators using the same alloy.

---

[1]J. Zhang
Materials Section
Department of Mechanical and Aerospace Engineering
University of California, Irvine, CA 92717
(714) 856-8583

1. INTRODUCTION

The effective utilization of advanced metals and alloys in structural applications that require minimal sound and vibration transmission is often limited by our current understanding of the factors that govern their microstructural damping response. The microstructural damping capacity of a material - referred to hereafter simply as damping capacity - may be defined as its ability to dissipate elastic strain energy, although plasticity may be involved at large strain amplitudes. The dissipation of elastic strain energy in the microstructure typically occurs through a combination of several mechanisms, which include: 1) relaxation of point defects, 2) macro-thermoelasticity, 3) micro-thermoelasticity, 4) Eddy-current effects, 5) Snoek effect, 6) stress-induced ordering reactions, and 7) electronic effects[1, 2]. In addition, the dissipation of elastic strain energy may be affected by discontinuities that may be present in the microstructure, such as grain boundaries and pores or cavities.[3-5]

There is a strong experimental evidence suggesting that the presence of pores or cavities in the microstructure may play an important role in the damping response of a material. Shimizu[3], for example, showed that the damping behavior of a carbon/epoxy composite could be modified either by adding a certain amount of flexibilizer or by foaming the epoxy matrix. His results demonstrated that the damping behavior of the carbon/epoxy composite samples was strongly influenced by the resulting porous microstructure that was induced during the foaming of the matrix. In related studies, Klimentos and McCann[4] investigated the relationship among compressional wave attenuation, porosity, clay content, and permeability in sandstones. In their study, they measured the attenuation coefficients of compressional waves of sandstone samples containing pores filled with clay and saturated with fluid. Their results showed that the logarithmic decrement (δ) of the samples at 1000 kHz and 40 MPa was related to porosity (P, in %) and clay content inside pore (C, in %) by $\delta = aP + bC - c$, where a, b and c are positive constants. They also noted that there was no apparent correlation between attenuation and mean grain size for their samples. Nielsen[5] developed a theoretical model to estimate the complex modulus of porous and impregnated materials (e.g. cement) and viscoelastic porous materials. Rice[6] also proposed a theoretical model to predict the effects of porosity and grain size on the tensile modulus, strength and fracture energy of ceramics.

Despite the aforementioned results which suggest that the presence of pores and cavities in the microstructure may have a strong influence on the overall damping response of a material, the understanding of the precise role played by pores and cavities in damping behavior is not clearly

understood. This lack of knowledge may limit efficient applications of certain advanced materials in damping-critical structures, since these materials often exhibit some amount of porosity. One of such class of materials includes, for example, that produced by powder metallurgical means (e.g., consolidating fine powders into bulk preforms).[7-8] Therefore, the objective of the present work is to provide insight into the effects of porosity on the damping behavior of structural aluminium alloys. Spray atomization and deposition processing was selected for the present study as a result of its ability to produce a material with a pre-determined amount of non-interconnected, micrometer-sized pores or cavities.[9-15] Furthermore, by using this synthesis approach, the amount and distribution of porosity present in the material may be systematically altered through variations in the processing parameters. Aluminum alloy 6061 was selected for the present study because it has been widely used in structural applications, and because its damping behavior has been studied previously.[2,16,17]

2. EXPERIMENTAL

2.1 MATERIAL SYNTHESIS

The aluminum alloy used in the present study was a commercial quality 6061 aluminum alloy, with the following nominal compositions: 0.6% Si, 0.28% Cu, 1.0% Mg, 0.2% Cr, and balance Al (in wt. %). Spray atomization and deposition processing involves the energetic disintegration of the molten 6061 alloy into micrometer-sized droplets by high velocity inert gas jets (N_2 was used in the present study), followed by deposition on a water cooled Cu substrate. The rapidly quenched, partially solidified droplets impact, first on the deposition surface, and subsequently on each other, and collect into a preform whose microstructure is largely dictated by the solidification conditions during impact. A diagram of the experimental apparatus used in the present study is shown in Figure 1. The geometry of the spray deposited material, which normally exhibits a contour akin to the Gaussian distribution of droplets impacting on the substrate,[9-13] was readily modified in the present study by displacing the substrate during deposition. In order to avoid extensive oxidation of the 6061 Al matrix during processing, the environmental chamber was evacuated to a pressure of 0.2 kPa, and backfilled with inert gas to pressure of 0.1 MPa prior to melting and atomizing the material. A more detailed discussion of the spray atomization and deposition experiments can be found elsewhere[9-15].

Two spray atomization and deposition experiments using 6061 Al were conducted for the present study. The primary experimental variables used during each experiment are shown in Table 1. The parameters in this table show that the metal to gas mass flow ratio, J_{melt}/J_{gas}, was the

only variable altered during the experiments. The effects of the melt to gas mass flow ratio used in Experiment 132, relative to that used in Experiment 134, on the resulting microstructure will be discussed in a subsequent section.

Table 1 Experimental Variables Used in the Study

Experiment number	132	134
Alloy	6061 Al	6061 Al
Atomization pressure	1.21 MPa	1.21 MPa
Atomization gas	nitrogen	nitrogen
Flight distance	40.64 cm	40.64 cm
Pouring temperature	750 °C	750 °C
Ratio of melt to gas mass flow rates	2.29	1.97

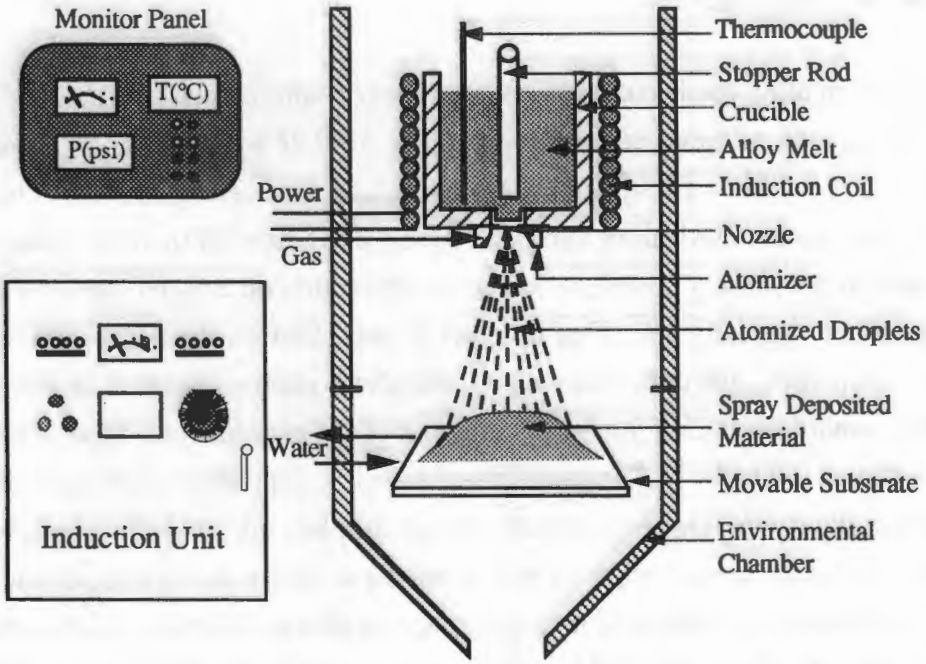

Figure 1. Schematic diagram showing spray atomization and deposition processing.

2.2 STRUCTURAL CHARACTERIZATION

The geometry of the spray atomized and deposited material is shown schematically in Figure 2. In this figure, the orientation of the Z axis was selected to lie in the height direction, whereas the orientation of the X and Y axes were chosen to lie in the short transverse and long

transverse directions, respectively. Cantilever beam specimens for damping characterization studies and samples for porosity analyses were simultaneously removed by sectioning the as-spray deposited material into rectangular bars. The following procedure was adopted in order to keep track of the precise location of each sample within the spray deposited material. The central core of the deposit was first sectioned into a block with the following approximate dimensions: 15 cm long x 7 cm wide x 6 to 8 cm high. This block was subsequently sectioned into several layers (usually 5 to 7 layers numbered with 1, 2, 3...7 from the bottom to the top) along the height direction, and

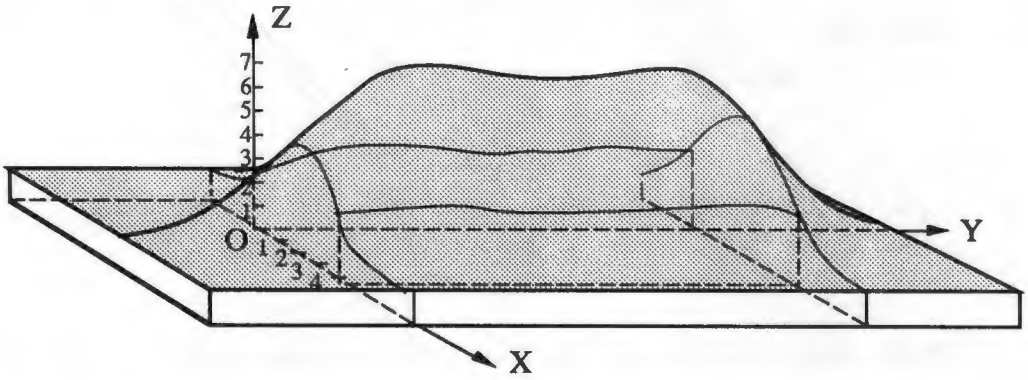

Figure 2. Schematic diagram showing the geometry of the as-spray deposited 6061 aluminum alloy.

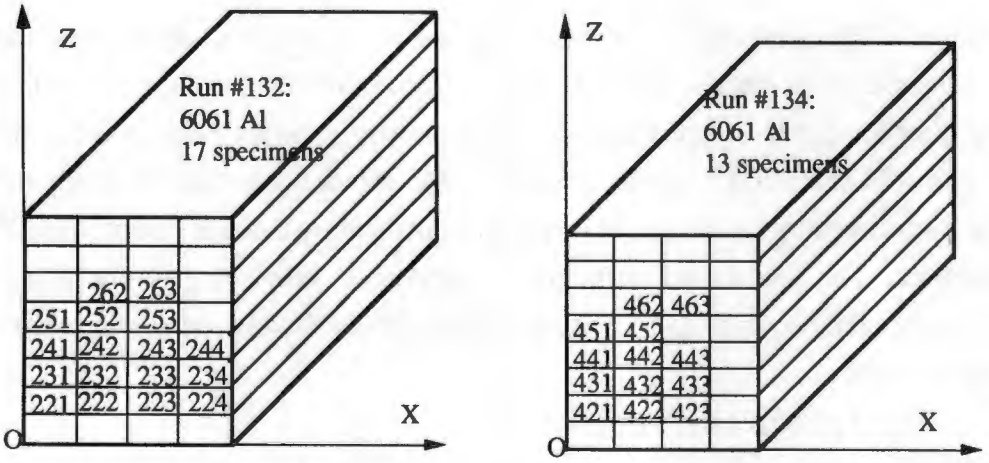

Figure 3. Schematic diagram showing position of samples within the as-spray deposited material.

each layer was then divided into rectangular samples (3 to 4 samples numbered 1, 2, 3 and 4). This procedure is shown schematically in Figure 3, for Experiments 132 and 134. In this figure, the relative location of each rectangular specimen inside the spray deposited block is designated by a number. Every rectangular sample was subsequently divided into two pieces; one was used for the damping measurements, and the other for porosity analyses (see Figure 4). This procedure

allowed careful analysis of the microstructure present in the damping specimens, since the microstructure of spray atomized and deposited materials has been reported to change with spray deposition thickness (Z axis), but remain relatively constant along the longitudinal dimension (Y axis).[18, 19]

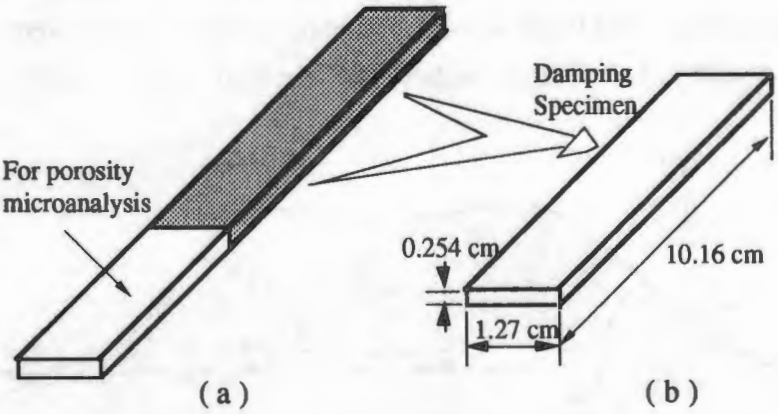

Figure 4. Schematic diagram showing specimen configuration and geometries.

2.3 POROSITY CHARACTERIZATION

Quantitative characterization of the porosity present in the spray deposited materials was accomplished by means of density measurements and computerized analysis of metallographic samples using an Imageset image analyzer. The density measurements were conducted in accordance with ASTM B311-83 Standard, based on Archimedes' principle. In this procedure the weight of each specimen in the air and in liquid was obtained by using a Fisher Scientific A-250 electronic balance. The liquid used in the present study was ethylene glycol with a density of 1.113 g/cm^3 at room temperature (25 °C). Accordingly, the density of specimen is calculated from the following equation

$$\rho_s = m_{sa}\,\rho_l / (m_{sa} - m_{sl}) \qquad (1)$$

where ρ_s and ρ_l denote the density of the specimen and the liquid, respectively, and m_{sa} and m_{sl} denote the mass of specimen in air and in liquid, respectively. It then follows that the amount of porosity present in each spray deposited sample can be determined by

$$P = (\rho_{Al} - \rho_s) / (\rho_{Al} - \rho_{gas}) \qquad (2)$$

where P denotes volume fraction of porosity present in sample material, ρ_{Al} represents the theoretical density of 6061 Al, and ρ_{gas} represents the density of any inert gas present inside the pores. In the present study, the density of extruded 6061 Al was used as the theoretical density, ρ_{Al}, and determined according to the following procedure. A 2.54 diameter cylinder was removed

from the as spray deposited 6061 Al, and extruded at 400 °C into a rod with a diameter of 1.27 cm; the extrusion pressure used was 27.58 MPa. The density of the extruded material was then determined according to Eq. (1) as $\rho_{Al} = 2.73$ g/cm^3. This value compares favorably with the measured density of 2.72 g/cm^3 for as-received 6061 Al. In view of the fact that the magnitude of ρ_{gas} is substantially smaller than that corresponding to ρ_{Al}, Eq. (2) is simplified, and P is calculated from the following equation

$$P = (\rho_{Al} - \rho_s) / \rho_{Al} \tag{3}$$

While the total amount of porosity present in the spray deposited materials was determined using the above described procedure, the distribution of pore sizes was quantitatively characterized for each specimen by using image analysis in combination with a Nikon Epiphot optical microscope and a Macintosh IIci computer. An adaptor was utilized in the present work to transmit images from the optical microscope directly to the computer, where the size distribution of pores was readily established. This procedure allowed the characterization of a large number of metallographic samples, accurately and efficiently.

2.4 DAMPING MEASUREMENTS

The cantilever beam technique was used in the present study to characterize the microstructural damping response of the spray deposited materials. In this technique, one end of a rectangular specimen was fixed in place while the opposite end was allowed move freely to respond to a mechanically induced displacement or vibration. The damping capacity of the material was then determined from the resulting displacement spectrum, by utilizing the logarithmic decrement and the half power band width analysis methodologies. In the logarithmic decrement method, a history of amplitude versus time during a free vibration of the cantilever beam specimen was recorded by an oscilloscope through an optical displacement transducer. By measuring the amplitude decay (Figure 5), the logarithmic decrement δ can be evaluated by

$$\delta = (1 / n) \ln (A_i / A_{i+n}) \tag{4}$$

where A_i and A_{i+n} are the amplitudes of the i^{th} cycle and the $(i+n)^{th}$ cycle at times t_1 and t_2, respectively, separated by n periods of oscillation.

The half power band width methodology is based on a forced vibration test in which the specimen was vibrated by a shaker which was driven by an amplified signal from a white noise generator. In this technique the resonant frequency peak is distinguished by recording the vibration amplitude as a function of frequency. The damping loss factor, η, may then be

calculated from the vibration spectrum, recorded by an FFT signal analyzer through an optical transducer using the following equation

$$\eta = (f_1 - f_2) / f_r \qquad (5)$$

where f_1, f_2 and f_r are shown in Figure 6. Finally, the logarithmic decrement, δ, and the loss factor, η, can be checked by the following relationship[2]

$$\eta = \delta / \pi \qquad (6)$$

All of the damping data used in the present study was derived from experiments performed at the Westinghouse Science and Technology Center (Pittsburgh, PA).

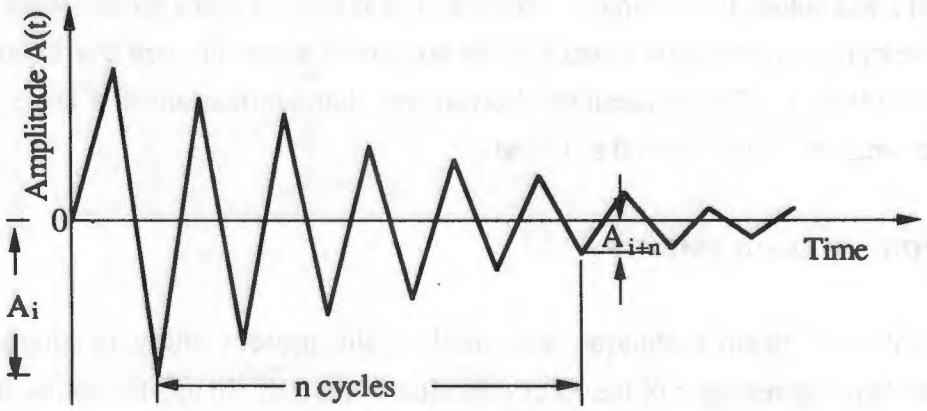

Figure 5. Schematic diagram of free vibration decay[2]

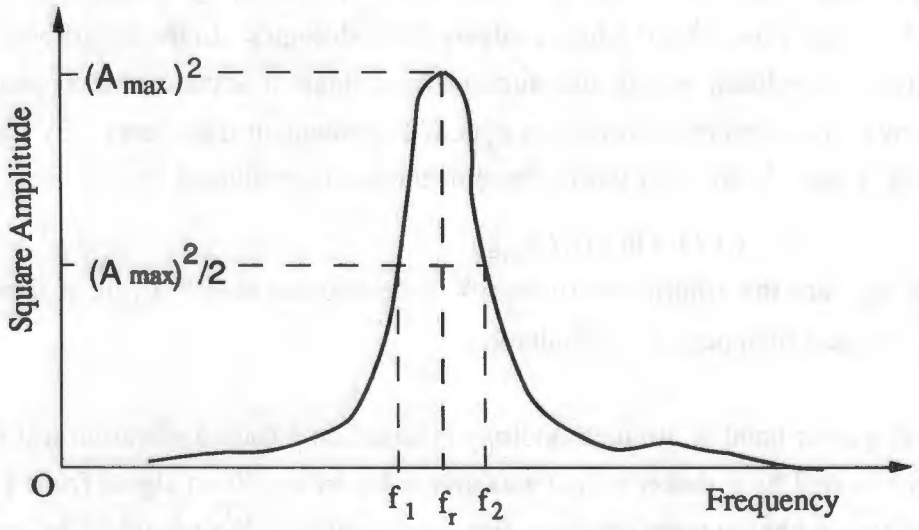

Figure 6. Schematic diagram showing Lorentzian Peak[2]

3. RESULTS

3.1 POROSITY AND MICROSTRUCTURE

Table 2 shows the density, ρ_s, and the amount of porosity, P, of the as-deposited 6061 Al specimens, calculated from Equations (1) and (3), respectively. The results shown in Table 2 correspond to the various locations within the spray deposited materials, as designated in Figure 3.

Table 2. Density and Porosity of As-Spray Deposited 6061 Al

Deposit	[1]Sample	m_{sa}(g)	m_{sl}(g)	ρ_s (g/cm^3)	P (%)
132	222	8.5844	4.8565	2.5606	6.20
132	242	8.5541	4.8380	2.5597	6.23
132	252	8.6848	4.9720	2.6011	4.72
132	234	8.3702	4.7875	2.5980	4.83
134	422	8.0587	4.4268	2.4674	9.61
134	442	7.5877	4.2314	2.5139	7.91
134	452	8.3760	4.6700	2.5132	7.94
134	433	8.3339	4.6130	2.4906	8.77

[1]Sample location is shown in Figure 3.

Optical microscopy was conducted on Keller's etched coupons of the as-spray deposited materials and two examples, corresponding to Experiments 132 and 134, are shown in Figures 7 and 8 respectively. The presence of numerous pre-solidified droplets in the microstructure precluded a precise quantitative assessment of the grain size. However, a large number of observations revealed that the as-spray deposited grain size ranges from 15 to 49 μm with a average of 32 μm for Deposit 132 and from 10 to 35 μm with a average of 22 μm for Deposit 134. In addition, it is worth noting that the microstructure remained relatively constant throughout the entire specimen length of the as-spray deposited materials. The evolution of microstructure during spray atomization and deposition has been addressed by numerous investigators, and the interested reader is encouraged to consult the available scientific literature.[10-15, 18]

The size distribution of the pores present in the samples from Deposits 132 and 134 are shown in Figures 9 and 10, respectively. In order to quantify the size distribution and morphology of the pores, optical metallography samples were studied using image analysis, in combination with a Nikon Epiphot optical microscope and a Macintosh IIci computer. The results are shown in Table 3, where the total amount of porosity present in the samples, as inferred from image analysis, is compared to that obtained using Archimedes' principle. Also shown in Table 3 is the average diameter of the pores present in the as-spray deposited microstructure, as determined from

image analysis. It is worth noting that each data point shown in Table 3 was determined by examining 2-3 viewing areas. This procedure increased the accuracy of the measured values. In general, comparison of the amount of porosity present in the spray deposited materials determined using image analysis and Archimede's principle revealed a relatively good agreement between both techniques.

Table 3 Porosity of As-Deposited 6061 Al by Image Analysis

Run	[1]Sample	P (%) by Image	P (%) by Archimede's	[2]d (μm)
132	222	6.45	6.20	5.38
132	242	6.90	6.23	3.96
132	252	4.80	4.72	2.36
132	234	3.78	4.83	1.91
134	422	10.12	9.61	9.30
134	442	8.99	7.91	7.32
134	452	7.42	7.94	5.51
134	433	9.48	8.77	5.50

[1]Sample location is shown in Figure 3.
[2]Average pore diameter as determined from image analysis.

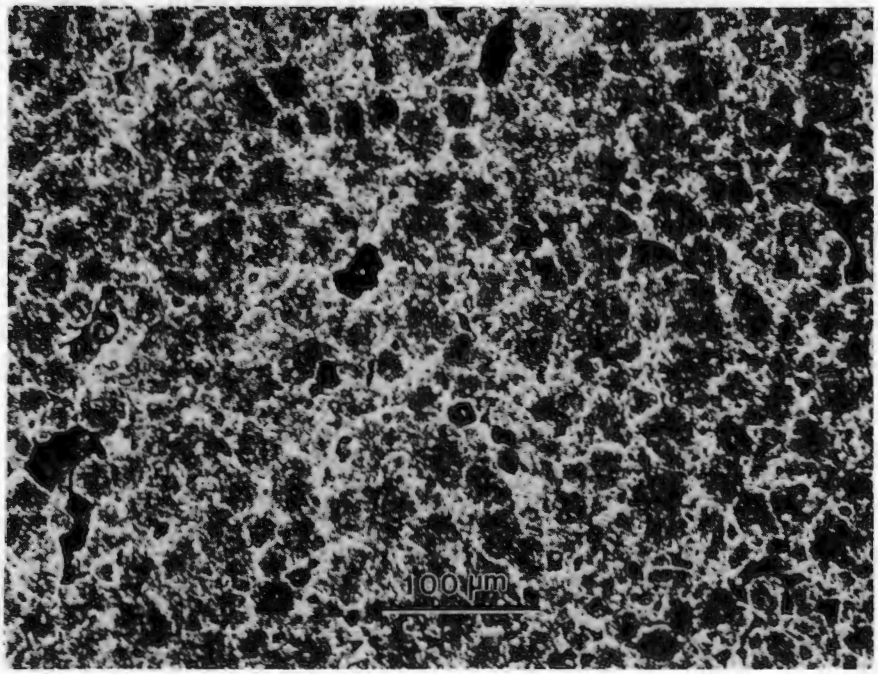

Figure 7. Optical micrograph showing the typical grain and pore morphology present in Deposit 132.

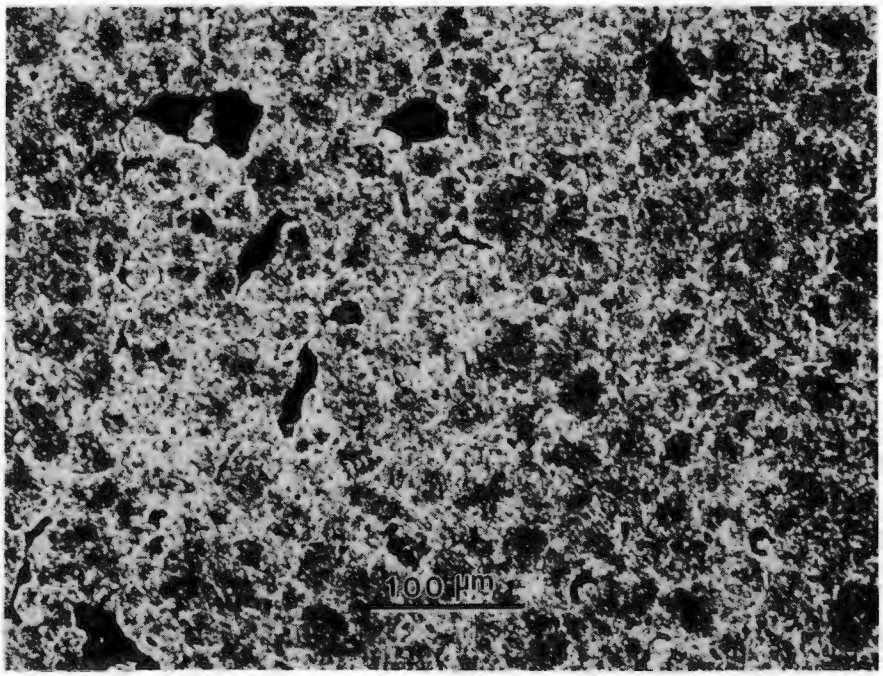

Figure 8. Optical micrograph showing the typical grain and pore morphology present in Deposit 134.

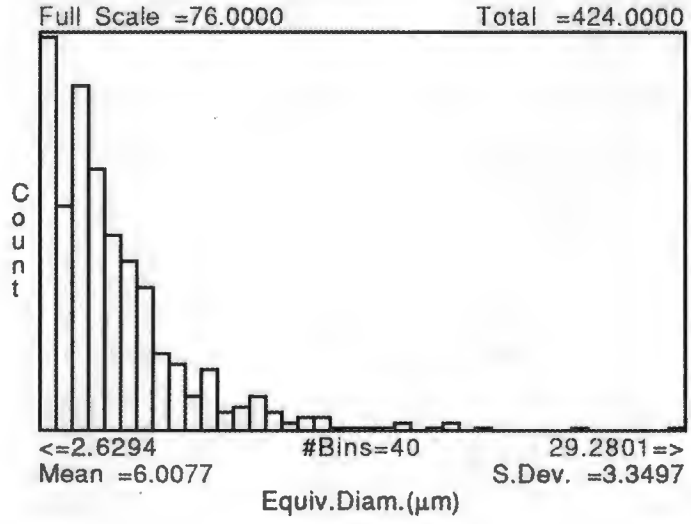

Figure 9. Distribution of pore sizes present in sample 222 (see Figure 3) from Deposit 132.

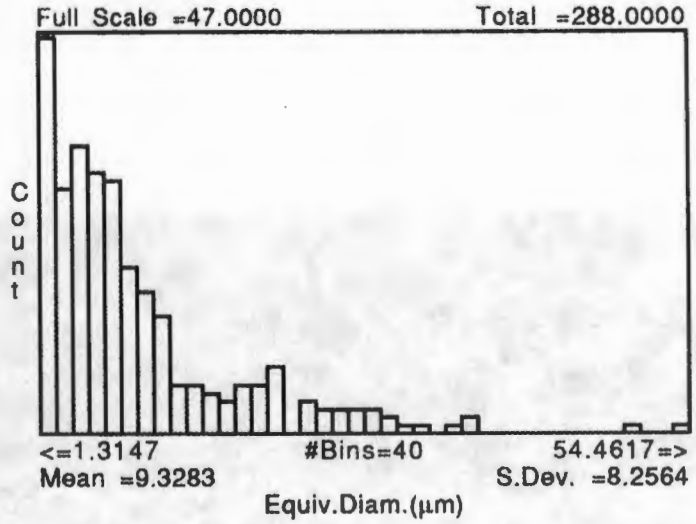

Figure 10. Distribution of pore sizes present in sample 422 (see Figure 3) from Deposit 134.

3.2 DAMPING CAPACITY

The damping response of the spray deposited materials, as determined from the experimental data in combination with Equations (4) and (5), are summarized in Table 4. Also shown in this table is the Lorentzian peak frequencies for each of the samples tested. It is worth noting that the free decay vibration tests were performed at a frequency of 220 Hz in order to allow comparison of the present data to that obtained by other investigators. Comparison of the values of the logarithmic decrement, δ, to those of the loss factor, η, using Eq. (6) suggests good agreement between the logarithmic decrement and the half power band width analysis methodologies. One notable exception to this observation is the result obtained for sample 442, which show that the loss factor for this sample was abnormally high (1.7). This was attributed to difficulties with the experimental measurements.

Table 4. Damping Capacity of As-Spray Deposited 6061 Al.

Deposit	Sample	δ (%)	f_r (Hz)	η (%)
132	222	2.0	294.50	0.7
132	242	1.9	292.00	0.6
132	252	1.9	300.25	0.6
132	234	2.0	287.50	0.7
134	422	2.9	280.75	0.8
134	442	2.6	261.25	1.7
134	452	1.8	281.25	0.8
134	433	2.3	280.50	0.8

4. ANALYSIS AND DISCUSSION

In order to discuss the effects of porosity on damping behavior it is first necessary to provide some background information on the factors that govern the formation of pores during spray atomization and deposition. This background information will also provide a basis for the discussion on the differences in the size and distribution of pores present in the materials obtained from Experiments 132 and 134. It is worth noting that since the present results showed that there was a relatively close correlation between the amount of porosity present and the average pore size (see Table 3), in the discussion that follows average pore size and amount of porosity may be thought of as interchangeable terms.

An important microstructural characteristic frequently associated with the microstructure of the as-spray atomized and deposited materials is the presence of a finite amount of non-interconnected pores.[9-15, 18, 22] The overall amount of porosity present in spray atomized and deposited materials depends on: (a) the thermodynamic properties of the material, (b) the thermodynamic properties of the gas, and (c) the processing parameters. Under conditions typical for aluminum alloys, for example, the amount of porosity present in spray atomized and deposited materials has been reported to be in the 1 to 10% range.[13, 14, 18] This is consistent with the results of the present study which showed the porosity levels in the 4 to 10% range. Furthermore, the present results also revealed that the size distribution of pores was skewed (see Figures 11 and 12), with an average pore diameter in the 6 to 10 μm range. It has been suggested that the origin of porosity in spray atomized and deposited materials may be attributed to one or a combination of the following mechanisms: (a) gas rejection, (b) solidification shrinkage, (c) interparticle porosity. The first mechanism, gas rejection, is anticipated as a result of the limited solid solubility of inert gases in most structural materials. As the temperature of the material decreases during solidification, any amount of gas that might have dissolved during the melting and superheating stage will be rejected into the matrix, leading to the formation of gas pores. However, results obtained using fast neutron activation analyses show that spray atomized and deposited materials exhibit extremely low levels of dissolved gases, suggesting that this mechanism is not as important as originally suggested.[23] In addition, in view of the irregular morphology of the pores, it is highly improbable that a large proportion of the porosity originates from the rejection of entrapped gases, since gas porosity generally exhibits a spheroidal morphology (see Figures 7 and 8).

The formation of shrinkage porosity is generally associated with sluggish solidification kinetics, such as those present during ingot casting. In view of the limited amount of liquid phase present under normal spray atomization and deposition conditions, it is unlikely that solidification

shrinkage plays an important role in the formation of the observed pore distribution.[13, 14, 21] It is worth noting, however, that if the spray atomization and deposition conditions are such that there is an excessive amount of liquid phase present at the deposition surface, this mechanism may play a significant role in the formation of porosity. The presence of excess amount of liquid phase during impact may develop as a result of (a) coarse droplet sizes, (b) high deposition temperatures, and (c) remelting of solid phases caused by high spray enthalpies.[13, 14] Under these conditions, the atomization gas may interact with the molten metal, leading to the formation of large amounts of porosity.

The available experimental evidence suggests that a large proportion of the porosity that is generally observed in spray atomized and deposited materials may be attributed to the third mechanism, interparticle porosity. As the droplets descend, first on the deposition surface, and eventually on each other, they overlap leaving micrometer-sized cavities in between. In spite of the large amount of turbulence present, the relatively rapid drop in temperature during deposition prevents any liquid phase present from filling all of the cavities, leading to the formation of irregular pores. This mechanism is consistent with the observed correlation between deposition conditions such as spray density, powder size, and the amount of porosity present throughout the deposit. For example, the higher density associated with the central region of the deposit may be attributed to the elevated mass flux of droplets in this region of the spray, relative to the periphery.[19] These droplets contain elevated fractions of liquid phase, effectively filling the interstices between droplets. Regarding the variations in density as a function of thickness, the present results show that the highest amount of porosity present in the spray deposited materials was present in the samples closest to the water cooled substrate (samples 222 and 422 in Table 3). This is consistent with the initially high rates of heat extraction experienced by the region of the deposit in close proximity to the substrate. In contrast, the high amount of porosity generally observed in the periphery of the samples (samples 234 and 433) results from a large proportion of small, presolidified droplets that tend to segregate to this region. It is noticed that under the processing conditions where deposited droplets are allowed to solidify completely before the arrival of more droplets, interlayer porosity will also develop at the original droplet boundaries.

In order to establish a relationship between the amount of porosity present and the processing parameters, it is useful to consider the factors governing the atomization stage of the process. The disintegration of a molten metal by high energy gas jets (atomization) is complex and only portions of it have been addressed from a theoretical viewpoint.[24] The work of Lubanska[25] has shown that the disintegration of liquids by high velocity jets obeys a simple correlation. A slightly modified form of the original correlation has been shown to represent the

results of molten metal atomization experiments reasonably well.[12, 20, 21] According to the modified Lubanska's correlation, the mass mean droplet diameter (i.e., the opening of a screening mesh which lets through 50 percent of the mass of the powder resulting from an atomization experiment), d_{50} is given by:

$$d_{50} = K_d [(\mu_m d_o \sigma_m / \mu_g V_{ge}^2 \rho_m) (1 + J_{melt} / J_{gas})]^{1/2} \quad (7)$$

where K_d is an empirically determined constant with a value between 40 and 400 (a value of 51.7 was selected for the conditions used in the present study, since this has been shown to yield a good correlation between theory and experiment[26]); μ_m, σ_m, ρ_m, and J_{melt} are the viscosity, surface tension, density and mass flow rate of the melt, respectively; μ_g, V_{ge}, and J_{gas} are the viscosity, velocity and mass flow rate of the atomizing gas, respectively; and d_o is the diameter of the metal delivery nozzle. Expressions for the flow rates can be obtained as functions of the process parameters from Bernoulli's equation in the case of the metal[27] and from theory of compressible flow[28] in the case of the gas. The mass mean droplet diameter of the powder size distribution (d_{50}) for both experiments was computed from Eq. (7), using the processing parameters and physical constants corresponding to each experiment (see Tables 1 and 5). Eq. 7 predicts d_{50} values of 108 μm and 98 μm for Experiments 132 and 134, respectively. These results are consistent with the higher densities that were noted for Experiment 132, relative to those of Experiment 134, since a smaller droplet diameter will dissipate thermal energy more effectively, thereby leading to a greater extent of pre-solidification prior to impact.

Table 5 Computational Results of d_{50} for Two Deposits of 6061 Al

Gas: Nitrogen			Melt: 6061 Al	
$\mu_g = 1.54 \times 10^{-4}$ g/cm·s			$\mu_m = 1.3 \times 10^{-2}$ g/cm·s	
$\rho_{gas} = 3.375 \times 10^{-3}$ g/cm³			$\rho_m = 2.385$ g/cm³	
$V_{ge} = 3.232 \times 10^4$ cm/s			$\sigma_m = 914$ g/s²	
$K_d = 51.7$				
Deposit	d_o	J_{gas}	J_{melt}	d_{50}
132	0.3048 cm	9.87 g/s	22.58 g/s	108 μm
134	0.2794 cm	9.87 g/s	19.46 g/s	98 μm

The damping capacity of the as-spray atomized and deposited 6061 Al obtained in the present study is summarized in Table 6, where the values of the logarithmic decrement, δ, are compared to the results obtained by other investigators using the same alloy. The values of the

logarithmic decrement, δ, shown in Table 6 were the average of the four samples investigated for each deposit (see Table 4). The results show that the value of δ of the spray atomized and deposited 6061 Al is higher than those reported by other investigators. The damping response of the spray atomized and deposited 6061 Al is thought to be derived from two factors: a) the presence of a finite amount of micrometer-sized pores, and b) a fine grained microstructure. In the discussion that follows, this suggestion is discussed in reference to results reported by other investigators.

Table 6. Comparison of Damping Behavior of 6061 to Results of other Studies.

Processing	Ref.	Experiment	Frequency	Amplitude	δ (%)
As-Deposited Run 132	This work	Cantilever beam	220 Hz	---	1.95±.05
As-Deposited Run 134	This work	Cantilever	220 Hz	---	2.40±.47
6061-T6	[16]	Cantilever	500 Hz	---	0.62
6061-T6	[17]	Cantilever	15 Hz	---	1.82
6061-T651	[2]	Cantilever	19.8 Hz	6-20x10^6ε	0.65

Previous studies[3-5] have demonstrated that the damping capacity of an impregnated porous material increases with the amount of porosity, concomitant with a drop in elastic modulus and strength. This observation is substantiated by the results obtained in the present study, as shown in Figure 11. The results shown in this figure suggest that the value of the logarithmic decrement, δ, increases with the percent of porosity present in the microstructure. The dissipation of elastic energy in porous materials has been rationalized in terms of a mechanism known as *mode conversion*.[29-31] From a macroscopic viewpoint, every point inside a cantilever beam specimen under lateral vibration will move in a transverse direction. Hence, every crystal or grain deforms in tension due to the transverse motion of the specimen and in shear due to the non-uniform deformation along longitudinal direction of the cantilever beam. In a porous metal, the tensile deformation may be converted into shear deformation at the boundaries of pores. The shear deformation may furthermore produce viscoelastic flow that is most readily achieved at the pore boundaries. The viscous flow is then converted to heat by molecular collisions or dislocations. The production of either thermal energy or dislocations are both beneficial to internal friction or material damping according to thermodynamics[32] and Granato-Lucke dislocation theory[33,34], respectively. The eventual result of these serial conversions is the decay of vibration inside the porous material.

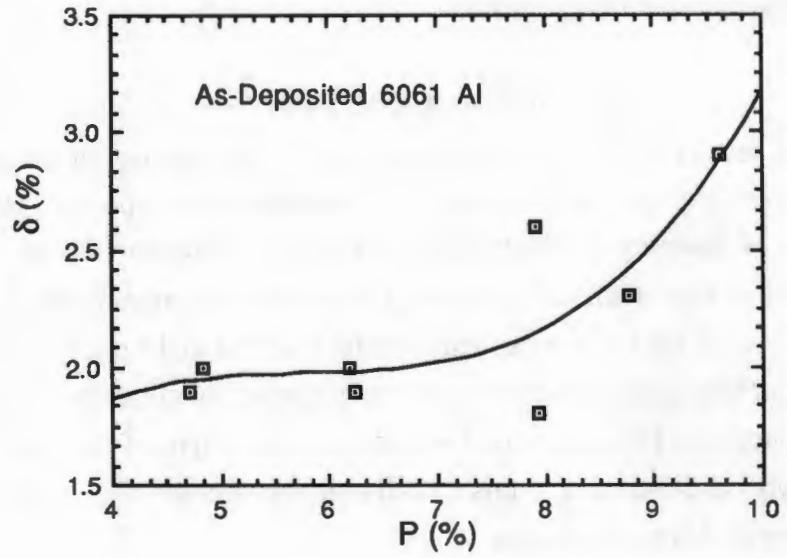

Figure 11. Relationship between damping capacity and porosity for as-deposited 6061 Al alloy.

Substantial mode conversion may be also reached when there is a certain medium inside the pores.[29] In the spray atomized and deposited 6061 material, and as discussed in a previous section, the low solutibity of the atomizing gas may lead to the formation of pores containing a partial pressure of inert gas. In this case, the motion of the inert gas relative to the porous framework material will be high, since the porous material is rigid in comparison with the inert gas. As a consequence, there will be an impedance mismatch to vibration movement between the inert gas and the as-spray deposited metal. This mismatch may change the deformation field in the neighboring metal region and therefore lead to secondary shear deformation in the neighboring metal, increasing the density of dislocations, and thereby the damping due to internal friction.

Damping associated with grain boundary relaxation, anelasticity or viscosity in the polycrystalline metals has been described by Zener,[35] Lazan[1] and Nowick[36], respectively. In polycrystalline metals there exist amorphous grain boundaries that display viscous-like properties. The viscous flow at grain boundaries will convert mechanical energy produced under cyclic shear stress into thermal energy, as a result of internal friction. The thermal energy will then be dissipated by the conductivity of metal and the heat exchange with the surroundings. The energy absorbed in grain boundaries not only depends on the magnitude of the shear stress and the anelastic shear strain, but also is proportional to the grain boundary area per unit volume, i.e., inersely proportional to grain size. In view of these results, the fine grained microstructure of the

spray atomized and deposited material may also play an important role in the dissipation of elastic strain energy. More detailed microstructural characterizations are currently under way in order to provide experimental basis for these suggestions.

5. CONCLUSIONS

In summary, the results of the present work show that the presence of micrometer-sized pores increases the damping capacity of the as-spray atomized and deposited 6061 Al alloy. Furthermore, the results of damping characterization studies show that the value of δ of the spray deposited 6061 Al is higher than the results reported by other investigators using the same alloy. The damping characteristics of the spray deposited material obtained in the present work is thought to be derived from two factors: a) the presence of a finite amount of micrometer-sized pores, and b) a fine grained microstructure. This suggestion was discussed in light of the relevant damping mechanisms. Further work is continuing in this area in order to ascertain the mechanisms that are responsible for the observed damping behavior.

6. ACKNOWLEDGEMENTS

The authors wish to acknowledge the Office of Naval Research (Grant No.: N00014-90-J-1923 to the University of California at Irvine, and Grant No.: N00014-90-C-0211 to the Westinghouse Science and Technology Center) for financial support. In addition, the authors would also like to express their gratitude to Catherine Wong of David Taylor Research Center, for her able technical assistance and valuable discussions; to E. S. Diaz of the Westinghouse Science and Technology Center and to I. Sauer of the University of California at Irvine for their assistance with the experimental part of this study; and to Y. Wu of the University of California at Irvine for his many insightful discussions.

REFERENCES

1. B.J. Lazan, Damping of Materials and Members in Structural Mechanics, Pergamon Press, Oxford, 1968.
2. G.G. Wren and V.K. Kinra, Damping in Metal Matrix Composites, Technical Report of Texas A&M University, 1990.
3. K. Shimizu, Composite Materials: Mechanics, Mechanical Properties and Fabrication, ed. by K. Kawata and T Akasaka, Japan Society for Composite Materials, Tokyo, 1981, p. 111.
4. T. Klimentos and C. McCann, Geophysics, 55(8), Aug. 1990, p. 998.

5. L.F. Nielsen, J. of the American Ceramics Society, **67**(2), 1984, p. 93.
6. R.W. Rice, Materials Science and Engineering, **A112**, 1989, p. 215.
7. S.M. Kaufman and S. Mocarski, Inter. J. of Powder Metallurgy, **7**, 1971, p. 19.
8. S.M. Kaufman, Inter. J. of Powder Metallurgy, **8**, 1972, p. 183.
9. P. S. Grant, W. T. Kim, B. P. Bewlay and B. Cantor, Scripta Metallurgica, **23**, 1986 p.1651.
10. A. L. Moran, and W. A. Palko, Journal of Metals, **40** (12),1988, p. 12.
11. P. Mathur, D. Apelian and A. Lawley, Acta Metallurgica, **37**, 1989, p.429.
12. E. Gutierrez, E. J. Lavernia, G. Trapaga, J. Szekely and N. J. Grant, Met. Trans., **20A**, 1989, p.71.
13. E.J. Lavernia, Inter. J. of Rapid Solidification, **5**, 1989, p. 47.
14. M. Gupta, F.A. Mohamed, and E.J. Lavernia, Inter. J. of Rapid Solidification, 1991, in press.
15. E.J. Lavernia, T. Ando and N.J. Grant, Proc. of ASM's 1986 International Conference on Rapidly Solidified Materials, San Diego, 1986, p. 29.
16. R.B. Bhagat, M.F. Amateau and E. C. Smith, Cast Reinforced Metal Composite, ed. by S.G. Fishman and A.K. Dhingra, ASM International, Materials Park, Ohio, 1988, p. 399.
17. M.S. Misra and P.D. LaGreca, Proc. of Vibration Damping 1984 Workshop Proceedings, AFWAL-TR-84-3064, Long Beach, Ca., Feb. 1984, p. U-1.
18. B.P. Bewley and B. Cantor, Proc. of 1st Inter. Conf. on Rapidly Solidified Materials, ed. by P. Lee and R. Carbonara, ASM International, Materials Park, Ohio, 1986, p.15.
19. V.G. McDonell, E.J. Lavernia and G.S. Samuelsen, Synthesis and Analysis in Materials Processing: Advances in Characterization and Diagnostics of Ceramic and Metal Particulate Processing, ed. by E.J. Lavernia, H. Henein and I. Anderson, The Metallurgical Society, 1989, p.30.
20. E.J. Lavernia et al., Proc. of the 1987 Annual Powder Metallurgy Conference and Exhibition, Progress in Powder Metallurgy, **43**, 1987, p. 683.
21. E. Gutierrrez, E.J. Lavernia, G. Trapaga, J. Szekely and N.J. Grant, Met. Trans., **20A**, 1989, p. 71.
22. R. Vetter, L. Z. Zhuang, I. Majewska-Glabus and J. Duszczyk, A Modified Spray Deposition Model Verified with Ni_3Al-Cr Intermetallic Alloys," Scripta Metall. et Mater., **24** (11), in press, 1990.
23. K. Ogata, E. J. Lavernia, G. Rai and N. J. Grant, International Journal of Rapid Solidification, **2** (1), 1986, p. 21.
24. T. Mikami, R.G. Cox and S.G. Mason, Int. J. Multiphase Flow, **2**, 1975, p. 113.
25. H. Lubanska, J. Metals, **22**, 1970, p. 45.

26. X. Zeng, Thesis for Master of Science in Engineering, University of California, Irvine, 1991.
27. G.H. Geiger and D.R. Poirier, Transport Phenomena in Metallurgy, Reading, MA, Addison-Wesley, 1973, p. 134.
28. A.H. Shapiro, The Dynamics and Thermodynamics of Compressible Fluid Flow, **1**, New York, NY, Ronald Press, 1953, p. 85.
29. Jacek Jarzynski, Sound and Vibration Damping with Polymers, American Chemical Society, Washington, DC, 1990, p.167.
30. R. D. Corsano et al., Ibid, p.208.
31. W.M. Madigosky and K.P. Sharnhorst, Ibid, p.228.
32. D. Zhang and B.I. Sandor, Fatigue Fract. Engng. Mater. Struc., **13**(5), 1990, p.497.
33. A. Granato and K. Lucke, J. of Appl. Phy., **27**(6), 1956, p.583.
34. A. Granato and K. Lucke, J. of Appl. Phy., **27**(7), 1956, p.789.
35. C. Zener, Elasticity and anelasticity of Metals, The University of Chicago Press, Chicago, IL., 1948, p.147.
36. A.S. Nowick and B.S. Berry, Anelastic Relaxation in Crystalline Solids, Academic Press, New York, 1972, p. 436.